

First-principles Study of the RKKY Interaction and the Quadrupole Order in the Pr 1-2-20 systems $\text{PrT}_2\text{Al}_{20}$ ($T=\text{Ti, V}$)

Yuto IIZUKA¹, Takemi YAMADA², Katsuro HANZAWA², and Yoshiaki ŌNO^{1*}

¹*Department of Physics, Niigata University, Niigata, 950-2181, Japan*

²*Department of Physics, Faculty of Science and Technology, Tokyo University of Science, Chiba, 278-8510, Japan*

Electronic states and quadrupole orders in the Pr 1-2-20 systems $\text{PrT}_2\text{Al}_{20}$ ($T=\text{Ti, V}$) are investigated on the basis of the first-principles calculations. The effective 196 orbital model is derived to reproduce the first-principles electronic structures of $\text{LaT}_2\text{Al}_{20}$ ($T=\text{Ti, V}$) without contribution from the Pr 4*f* electrons which are considered to be well localized and is employed to calculate the Ruderman-Kittel-Kasuya-Yosida (RKKY) interactions between quadrupole and octupole moments of the Pr ions. Within the random phase approximation for the RKKY Hamiltonian, the most divergent susceptibility is found to be the quadrupole one for the wave vector $\mathbf{Q} = (0, 0, 0)$ in the case of $\text{PrTi}_2\text{Al}_{20}$ while that for $\mathbf{Q} = (\pi/a, 0, \pi/a)$ in the case of $\text{PrV}_2\text{Al}_{20}$ as consistent with experimental observations in the both cases which exhibit the ferro-quadrupole (FQ) and the antiferro-quadrupole (AFQ) orders, respectively. We also discuss the ordered states using the mean-field approximation and find that, in the case of $\text{PrTi}_2\text{Al}_{20}$, the 1st-order phase transition to the O_2^0 FQ order with a tiny discontinuity takes place as predicted by the Landau theory. In the case of $\text{PrV}_2\text{Al}_{20}$, the system exhibits two distinct O_2^2 AFQ orders, AFQ-I and AFQ-II, and shows subsequent two phase transitions, the 2nd-order one from normal to AFQ-I and the 1st-order one from AFQ-I to AFQ-II, that may be responsible for the double transitions observed by specific heat measurements.

arXiv:2203.15281v1 [cond-mat.str-el] 29 Mar 2022

1. Introduction

Recently, the Pr 1-2-20 systems $\text{PrT}_2\text{X}_{20}$ have attracted much attention as they show various interesting phenomena including quadrupole orders, superconductivity and non Fermi liquid behaviors.¹⁾ The crystal structure is the cubic $\text{CeCr}_2\text{Al}_{20}$ -type with the space group $\text{Fd}\bar{3}\text{m}$,²⁾ where the Pr atoms are encapsulated in the Frank-Kasper cages formed by 16 X atoms³⁾ and are under T_d -symmetry. The crystalline electric field (CEF) ground states of the Pr ions with the 4*f*² configuration are the non-Kramers doublets Γ_3 , where we can elucidate the effects of the electric quadrupoles without taking into account of the magnetic moments.

In fact, $\text{PrTi}_2\text{Al}_{20}$ exhibits the ferro-quadrupole (FQ) order below the transition temperature $T_Q = 2.0 \text{ K}$,^{4,5)} at the ambient pressure, and $\text{PrV}_2\text{Al}_{20}$, $\text{PrIr}_2\text{Zn}_{20}$ and $\text{PrRh}_2\text{Zn}_{20}$ exhibit the antiferro-quadrupole (AFQ) order below $T_Q = 0.6, 0.11$ and 0.06 K , respectively.⁶⁻⁹⁾ Among them, the ordered quadrupole moments have been determined as O_2^0 for the FQ order in $\text{PrTi}_2\text{Al}_{20}$ ^{10,11)} while O_2^2 for the AFQ order in $\text{PrIr}_2\text{Zn}_{20}$.¹²⁾ In addition, high-quality single crystals in $\text{PrV}_2\text{Al}_{20}$ exhibit remarkable double transitions at $T_Q = 0.75 \text{ K}$ and $T^* = 0.65 \text{ K}$ ¹⁵⁾ below which another quadrupole and/or octupole order is expected to be realized. More recently, the FQ order of $\text{PrTi}_2\text{Al}_{20}$ has been found to show magnetic-field-induced 1st-order phase transitions^{16,17)} which are well reproduced by the Landau theory based on the mean-field approximation.¹⁸⁾

As is well known, the details of the energy band dispersions near the Fermi level responsible for the Fermi surfaces are important to discuss what kinds of ordered states including quadrupole one take place. In the 1-2-20 systems, the de Haas-van Alphen (dHvA) experiments revealed that the Fermi surfaces for $\text{PrTi}_2\text{Al}_{20}$ and $\text{PrIr}_2\text{Zn}_{20}$ are well accounted for by the first-principles band calculations for $\text{LaTi}_2\text{Al}_{20}$ and $\text{LaIr}_2\text{Zn}_{20}$ without contribution from 4*f* electrons of

Pr ions, respectively,^{19,20)} which is interpreted as indicating that the 4*f* electrons are sufficiently localized. Then, the quadrupole order of the localized 4*f* electrons is considered due to the Ruderman-Kittel-Kasuya-Yosida (RKKY) interaction²¹⁻²³⁾ between the quadrupole moments of Pr ions mediated by the conduction (*c*) electrons, where details of the electronic structure of the *c* electrons are important to determine the RKKY interaction.^{24,25)}

In the previous paper,²⁶⁾ we have calculated the RKKY interaction between the quadrupole moments of the Pr ions in $\text{PrT}_2\text{Al}_{20}$ ($T=\text{Ti, V}$) on the basis of the realistic tight binding models for the *c* electrons extracted from the first-principles band calculation and have found that the wave vector of the expected quadrupole order is $\mathbf{Q} = (0, 0, 0)$ in the case of $\text{PrTi}_2\text{Al}_{20}$ while it is $\mathbf{Q} = (\pi/a, 0, \pi/a)$ in the case of $\text{PrV}_2\text{Al}_{20}$ as consistent with experimental observations in $\text{PrTi}_2\text{Al}_{20}$ and $\text{PrV}_2\text{Al}_{20}$ which exhibit FQ and AFQ orders, respectively. The effects of the octupole moments and the ordered states below T_Q , however, were not considered there.²⁶⁾ The present paper is a straight-forward extension of our previous work²⁶⁾ to include the RKKY interaction between the octupole moments in addition to the quadrupole ones and to explicitly discuss the ordered states below T_Q , that is important for comparison with the experiments.

2. Model and Formulation

First, we perform the first-principles band calculations for $\text{LaT}_2\text{Al}_{20}$ ($T=\text{Ti, V}$) on the basis of the density-functional theory (DFT) with the generalized gradient approximation (GGA) by using WIEN2k code,²⁷⁾ where $17 \times 17 \times 17$ *k*-points, the muffin-tin radius $R_{\text{MT}} = 2.5$ (2.3) a.u. for La and T (Al) and the plane-wave cutoff $K_{\text{max}} = 3.2$ (a.u.)⁻¹ are used. As for the lattice parameters, we employ the experimentally determined values of $\text{PrT}_2\text{Al}_{20}$ ($T=\text{Ti, V}$)²⁸⁾ instead of $\text{LaT}_2\text{Al}_{20}$ in order to discuss the former electronic states in the 4*f* electron localized regime. In addition, we use the

*E-mail address: y.ono@phys.sc.niigata-u.ac.jp

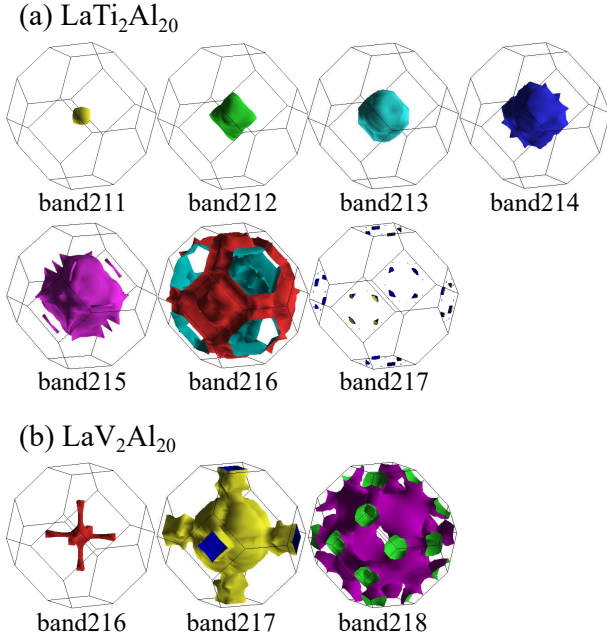


Fig. 1. (color online) Fermi surfaces of (a) $\text{LaTi}_2\text{Al}_{20}$ and (b) $\text{LaV}_2\text{Al}_{20}$ from the first-principles band calculations, where band211-215 in (a) and band216 in (b) are hole Fermi surfaces and the others are electron ones.

GGA+ U method with an artificially large value of $U = 60$ eV to exclude the La-4 f components near the Fermi level. Figures 1 (a) and (b) show the obtained Fermi surfaces of $\text{LaT}_2\text{Al}_{20}$ ($T=\text{Ti}, \text{V}$) which are in good agreements with those in the previous studies.^{19,29}

Next, we derive the tight binding models for the conduction electrons so as to reproduce the first-principles electronic structures near the Fermi level for $\text{LaT}_2\text{Al}_{20}$ ($T=\text{Ti}, \text{V}$) as shown in Figs. 2 (a) and (b), respectively, by using the maximally localized Wannier functions³⁰ which consist of 196 orbitals as a primitive unit cell includes $\text{La}_2\text{T}_4\text{Al}_{40}$: La- d (5 orbitals \times 2 sites), La- s (1 orbital \times 2 sites), T - d (5 orbitals \times 4 sites), T - s (1 orbital \times 4 sites), Al- p (3 orbitals \times 40 sites) and Al- s (1 orbital \times 40 sites) in the conventional unit cell.²⁶ When Ti is substituted by V in $\text{PrT}_2\text{Al}_{20}$ ($T=\text{Ti}, \text{V}$), the number of electron increases and then the Fermi level shifts upward as shown in Figs. 2 (a) and (b) resulting in the disappear of the small hole FSs of the band211-214 centered at the Γ point (see Fig. 1 (a)) which are crucial for a ferro-component of the susceptibility in the case of $\text{PrTi}_2\text{Al}_{20}$ as mentioned later.

The RKKY interaction between the localized f electrons is the indirect interaction mediated by the c electrons via the hybridization between the c and f electrons.²¹⁻²³ As the Pr 5 d electrons give the dominant contribution to the susceptibility responsible for the RKKY interaction, we consider the c - f hybridization only between the 5 d and 4 f on the same Pr atom which becomes finite for the CEF Hamiltonian \mathcal{H}_{CEF} without inversion symmetry³¹ and is explicitly given by

$$V_{mm'\ell\sigma}^{(n)} = \langle f^n m | \mathcal{H}_{\text{CEF}} | f^{n-1} m' \rangle | \ell \sigma \rangle, \quad (1)$$

where $|f^n m\rangle$ is a state of the Pr 4 f^n configuration labeled by m and $|\ell\sigma\rangle$ is a Pr 5 d state with the orbital ℓ and spin σ , where the t_{2g} orbital exclusively hybridizes with the f orbital in the case with the T_d -symmetric CEF Hamiltonian. The explicit

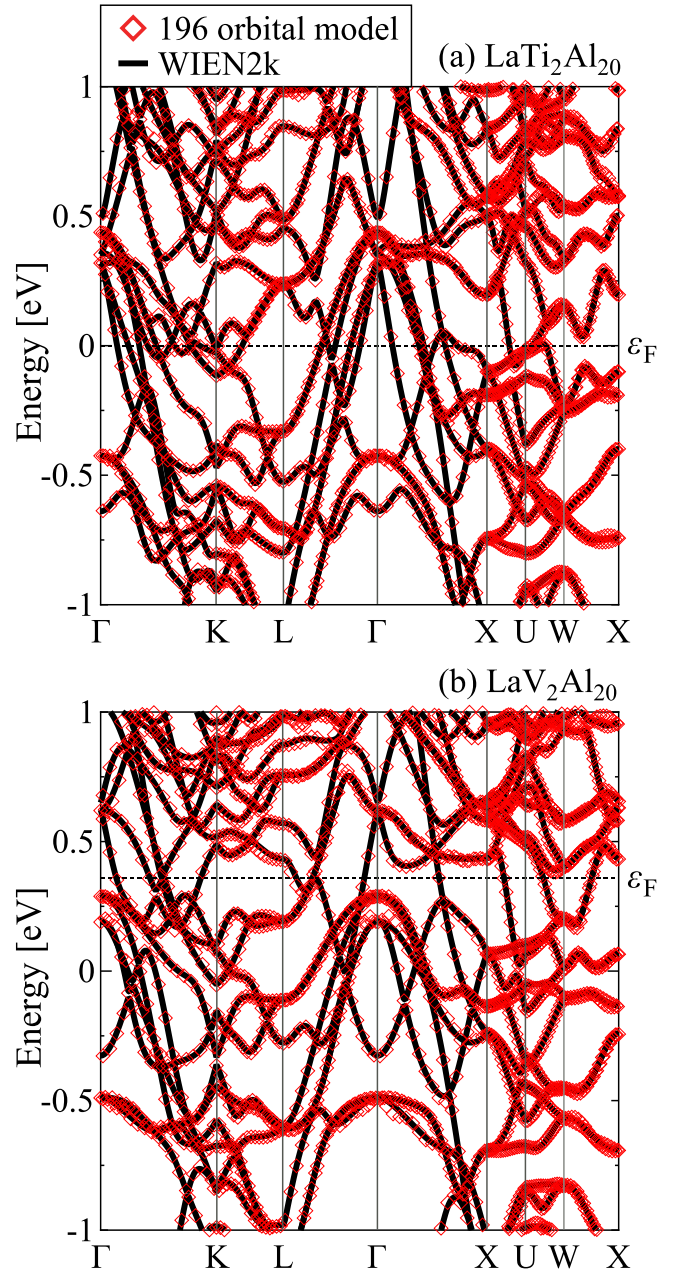


Fig. 2. (color online) Energy band dispersions near the Fermi level ϵ_F (black dashed line) of $\text{LaTi}_2\text{Al}_{20}$ (a) and $\text{LaV}_2\text{Al}_{20}$ (b) from the 196 orbital models (red diamonds) together with those from the first-principles band calculations using WIEN2k (black solid lines) as functions of the wave vector along the symmetric lines through the following symmetric points: Γ : (0, 0, 0), K : $(3\pi/4a, 3\pi/4a, 3\pi/2a)$, L : $(\pi/a, \pi/a, \pi/a)$, X : $(\pi/a, 0, \pi/a)$, U : $(5\pi/4a, \pi/2a, 5\pi/4a)$ and W : $(\pi/a, \pi/2a, 3\pi/2a)$, where the energies are plotted relative to the Fermi level of $\text{LaTi}_2\text{Al}_{20}$ in the both (a) and (b) and $\epsilon_F = 0.38\text{eV}$ in (b) indicates the relative shift of the Fermi level of $\text{LaV}_2\text{Al}_{20}$.

dependence of $V_{mm'\ell\sigma}^{(n)}$ on m, m', ℓ and σ is determined by using the Clebsch-Gordan coefficients²⁴ (not shown) except for the absolute value proportional to the strength of the CEF potential V_{CEF} which is an unknown parameter here.

In the non-Kramers doublet ground states Γ_3 of Pr 4 f^2 , the second-order perturbation with respect to $V_{mm'\ell\sigma}^{(n)}$ yields the Kondo exchange interaction Hamiltonian

$$H_{\text{ex}} = \sum_i \sum_{\mu=1,2} \sum_{\alpha=x,y,z} \sum_{\ell\ell'=t_{2g}} \sum_{\sigma\sigma'=\uparrow,\downarrow} K_{\ell\ell'\sigma\sigma'}^\alpha \hat{X}_\alpha^\mu(i) d_{iv\ell\sigma}^\dagger d_{iv\ell'\sigma'}, \quad (2)$$

where $d_{i\nu\ell\sigma}^\dagger$ is the creation operator for a Pr $5d-t_{2g}$ electron with orbital ℓ and spin σ at Pr site μ of the i -th unit cell, and \hat{X}_α is the multipole operator explicitly defined as follows: the quadrupoles O_2^0 for $\alpha = z$ and O_2^2 for $\alpha = x$ and the octupole T_{xyz} for $\alpha = y$. In eq. (2), the Kondo coupling is given by

$$K_{\ell\ell'\sigma\sigma'}^\alpha = \frac{1}{2} \sum_{mm'\in\Gamma_3} \sum_M \langle f^2 m' | \hat{X}_\alpha | f^2 m \rangle \times \left(D_+ V_{Mm\ell\sigma}^{(3)*} V_{Mm'\ell'\sigma'}^{(3)} + D_- V_{m'M\ell\sigma}^{(2)*} V_{mM\ell'\sigma'}^{(2)} \right) \quad (3)$$

with

$$D_+ = 1/(E_M^{(3)} - E_m^{(2)} - \varepsilon_F), \quad (4)$$

$$D_- = 1/(\varepsilon_F + E_M^{(1)} - E_m^{(2)}), \quad (5)$$

where $E_m^{(2)}$ and $E_M^{(3)}$ are the energies for the state m of the Pr $4f^2$ with the non-Kramers doublets Γ_3 and the state M of the Pr $4f^{1(3)}$ with $J = 5/2$ ($9/2$), and ε_F is the Fermi level around which the energy bands largely consist of Pr $5d-t_{2g}$ orbitals exist. Among the energies, $E_M^{(1)}$ and ε_F can be extracted from the first-principles band calculation, but $E_m^{(2)}$ and $E_M^{(3)}$ including the effects of the Coulomb interaction between the Pr $4f$ electrons are not explicitly determined here.

From the second-order perturbation with respect to H_{ex} in eq. (2), we obtain the RKKY Hamiltonian between the quadrupoles $\hat{X}_z = \hat{O}_2^0$ and $\hat{X}_x = \hat{O}_2^2$ and the octupole $\hat{X}_y = \hat{T}_{xyz}$ at the Pr site $\mu(\nu)$ of the $i(j)$ -th unit cell as

$$H_{\text{RKKY}} = - \sum_{(i,j)} \sum_{\mu\nu=1,2} \sum_{\alpha\beta=x,y,z} J_{\alpha\beta}^{\mu\nu}(i,j) \hat{X}_\alpha^\mu(i) \hat{X}_\beta^\nu(j), \quad (6)$$

with the RKKY interaction given by

$$J_{\alpha\beta}^{\mu\nu}(i,j) = \frac{1}{N} \sum_{\mathbf{q}} \sum_{\{\ell\}} \sum_{\sigma\sigma'} K_{\ell_1\ell_2\sigma\sigma'}^\alpha K_{\ell_3\ell_4\sigma\sigma'}^{\beta*} \chi_{\ell_1\ell_2\ell_3\ell_4}^{\mu\nu}(\mathbf{q}) e^{i\mathbf{q}\cdot(\mathbf{r}_i-\mathbf{r}_j)}, \quad (7)$$

where \mathbf{q} is the wave vector, \mathbf{r}_i is the position of the i -th unit cell and N is the total number of the unit cell. In eq. (7), the susceptibility for the c electrons is given by

$$\chi_{\ell_1\ell_2\ell_3\ell_4}^{\mu\nu}(\mathbf{q}) = \frac{1}{N} \sum_{\mathbf{k}s s'} u_{\ell_1 s}^{\mu*}(\mathbf{k}) u_{\ell_2 s'}^{\mu*}(\mathbf{k} + \mathbf{q}) u_{\ell_3 s}^{\nu*}(\mathbf{k}) u_{\ell_4 s'}^{\nu*}(\mathbf{k} + \mathbf{q}) \times \frac{f(\varepsilon_{s'}(\mathbf{k} + \mathbf{q})) - f(\varepsilon_s(\mathbf{k}))}{\varepsilon_s(\mathbf{k}) - \varepsilon_{s'}(\mathbf{k} + \mathbf{q})}, \quad (8)$$

where $\varepsilon_s(\mathbf{k})$ is the energy for the c electrons with the wave vector \mathbf{k} and the band s and $u_{\ell s}(\mathbf{k})$ is the corresponding eigen vector of the component of the orbital ℓ , and $f(\varepsilon)$ is the Fermi distribution function.

3. Results

Substituting $\varepsilon_s(\mathbf{k})$ and $u_{\ell s}(\mathbf{k})$ obtained from the 196 orbital models into eq. (8), we calculate the RKKY interaction eq. (7) with eqs. (3) and (8), where we set temperatures $T = 0.01 - 0.05$ eV around and below which $\chi_{\ell_1\ell_2\ell_3\ell_4}^{\mu\nu}(\mathbf{q})$ is found to be almost independent of T . We note that the 196 orbital models are necessary to obtain $u_{\ell s}(\mathbf{k})$, although $\varepsilon_s(\mathbf{k})$ can be obtained directly from the first-principles band calculations. In order to evaluate the Kondo coupling in eq. (3), there are two individual unknown parameters D_+ and D_- in which the effect of another unknown parameter, the strength of V_{CEF} , can be included. Hereafter, we set the value of D_-

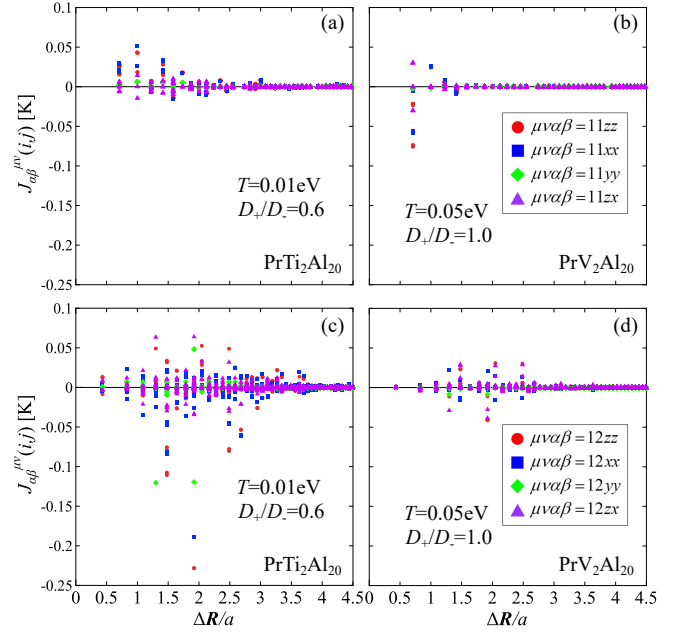


Fig. 3. (color online) Spatial dependence of the RKKY interactions of the diagonal components for O_2^0 ($\alpha\beta = zz$), O_2^2 ($\alpha\beta = xx$) and T_{xyz} ($\alpha\beta = yy$) and those of the off-diagonal component of $O_2^0-O_2^2$ ($\alpha\beta = zx$) between the same Pr sites $\mu = \nu = 1$ (a)(b), and those between the different Pr sites $\mu = 1$ and $\nu = 2$ (c)(d) in the cases of PrTi₂Al₂₀ (a)(c) and PrV₂Al₂₀ (b)(d), respectively, where $\Delta\mathbf{R} \equiv |\mathbf{R}_i^\mu - \mathbf{R}_j^\nu|$ with the position \mathbf{R}_i^μ of the Pr ion at site μ of the i -th unit cell and $a = 14.725\text{\AA}$ (14.567\AA) is the lattice constant for PrTi₂Al₂₀ (PrV₂Al₂₀).

with keeping the ratio $D_+/D_- = 0.6$ (1.0)³²⁾ so as to reproduce the experimentally observed transition temperature T_Q of the FQ (AFQ) for PrTi₂Al₂₀ (PrV₂Al₂₀) within the mean-field approximation for the RKKY Hamiltonian eq. (6).

Figures 3 (a)-(d) show the RKKY interactions $J_{\alpha\beta}^{\mu\nu}(i,j)$ as functions of the relative distance $\Delta\mathbf{R}$ between the Pr ions in the cases of PrTi₂Al₂₀ ((a) and (c)) and PrV₂Al₂₀ ((b) and (d)), respectively, where the parameters T and D_+/D_- are set as mentioned in the preceding paragraph. We observe that $J_{\alpha\beta}^{\mu\nu}(i,j)$ exhibit oscillatory decreases with $\Delta\mathbf{R}$ more than four unit cells (62th nearest neighbor sites). As shown in Fig. 3 (a) and (b), the diagonal components for the quadrupoles O_2^0 and O_2^2 between the nearest neighbor sites are positive (negative) responsible for the same (opposite) sign of the quadrupoles yielding the FQ (AFQ) order in the case of PrTi₂Al₂₀ (PrV₂Al₂₀). We note that, not only the diagonal components for the quadrupoles O_2^0 and O_2^2 but also the diagonal component for the octupole T_{xyz} and the off-diagonal components between O_2^0 and O_2^2 have significant values as shown in Figs. 3 (c) and (d).³³⁾

To discuss the expected multipole orders and the wave vectors \mathbf{q} of the ordered states, we perform the Fourier transformation of the RKKY interaction. Figures 4 (a)-(b) show the \mathbf{q} -dependence of the Fourier transformed RKKY interactions $J_{\alpha\beta}^{\mu\nu}(\mathbf{q})$ in the cases of PrTi₂Al₂₀ ((a) and (c)) and PrV₂Al₂₀ ((b) and (d)), respectively, where the parameters T and D_+/D_- are the same as those in Figs.3 (a)-(d). We find that the diagonal components for the quadrupoles has a maximum at $\mathbf{Q} = (0, 0, 0)$ in the case of PrTi₂Al₂₀ (see Fig. 4 (a)) and at $\mathbf{Q} = (\pi/a, 0, \pi/a)$ in the case of PrV₂Al₂₀ (see Fig. 4 (b)),

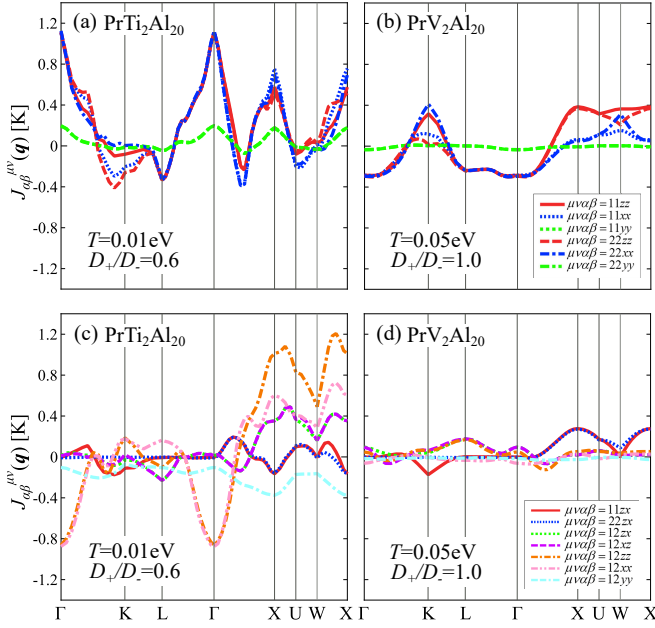


Fig. 4. (color online) Fourier transforms of the RKKY interactions of diagonal components (a)(b) and off-diagonal components with respect to the multipoles and/or the Pr sites (c)(d) in the cases of $\text{PrTi}_2\text{Al}_{20}$ (a)(c) and $\text{PrV}_2\text{Al}_{20}$ (b)(d), respectively, as functions of the wave vector along the symmetric lines through the symmetric points as the same as in Fig. 2. We note that the off-diagonal components of $J_{\alpha\beta}^{\mu\nu}(\mathbf{q})$ are generally complex and only the real parts are plotted in (c) and (d).

while the diagonal component for the octupole is smaller than the quadrupole components. Within the RPA, these results indicate that the FQ and the AFQ orders take place in the cases of $\text{PrTi}_2\text{Al}_{20}$ and $\text{PrV}_2\text{Al}_{20}$, respectively, as consistent with experimental observations. We note that the other subdominant contributions such as the diagonal components for O_2^0 and O_2^2 between the intersite $\mu = 1$ and $\nu = 2$ in the case of $\text{PrTi}_2\text{Al}_{20}$ (see Fig. 4 (c)) and the off-diagonal components between O_2^0 and O_2^2 at the same site in the case of $\text{PrV}_2\text{Al}_{20}$ (see Fig. 4 (d)) are also important to determine the ordered states below T_Q as shown later.

As the RKKY interactions obtained in the present study are long-range interactions between more than 62th nearest neighbor sites (see Figs. 3 (a)-(d)), the ordered states are expected to be described well with the mean-field approximation in contrast to the simplified models with the nearest neighbor interactions. Then, we solve the RKKY Hamiltonian eq. (7) with the obtained RKKY interactions within the mean-field approximation and find that the FQ and the AFQ orders take place in the cases of $\text{PrTi}_2\text{Al}_{20}$ and $\text{PrV}_2\text{Al}_{20}$, respectively, as shown in Figs. 5 (a) and (b), where the order parameters of the i -th unit cell are given by $\langle \hat{X}_\alpha^\mu(i) \rangle = \langle \hat{X}_\alpha^\mu \rangle$ for the FQ order and $\langle \hat{X}_\alpha^\mu(i) \rangle = \langle \hat{X}_\alpha^\mu \rangle e^{i\mathbf{Q} \cdot \mathbf{R}_i}$ with $\mathbf{Q} = (\pi/a, 0, \pi/a)$ for the AFQ order. We have no octupole moment $\langle \hat{T}_{xyz} \rangle$ in the both cases of $\text{PrTi}_2\text{Al}_{20}$ and $\text{PrV}_2\text{Al}_{20}$ as consistent with the μSR experiments.^{34,35)}

In the case of $\text{PrTi}_2\text{Al}_{20}$ shown in Fig. 5 (a), the order parameter changes its sign between the Pr site 1 and 2 in the same unit cell, that is due to the negative value of the site-off-diagonal components of the RKKY interactions at $\mathbf{q} = (0, 0, 0)$ as shown in Fig. 4 (c). The linear combinations of the obtained order parameters $\langle \hat{O}_2^0 \rangle$ and $\langle \hat{O}_2^2 \rangle$ yield the O_2^0 -

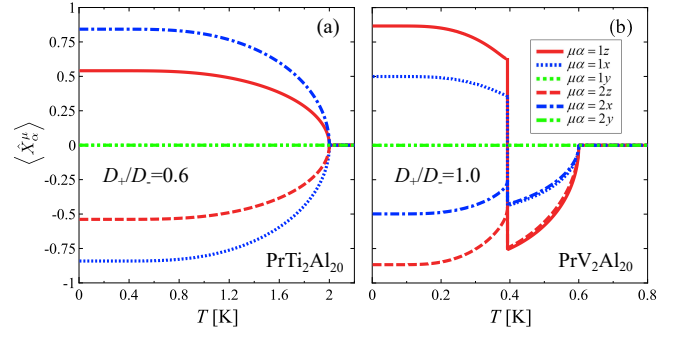


Fig. 5. (color online) Temperature dependence of the order parameters for the FQ order in the case of $\text{PrTi}_2\text{Al}_{20}$ (a) and that for the AFQ order in the case of $\text{PrV}_2\text{Al}_{20}$ (b).

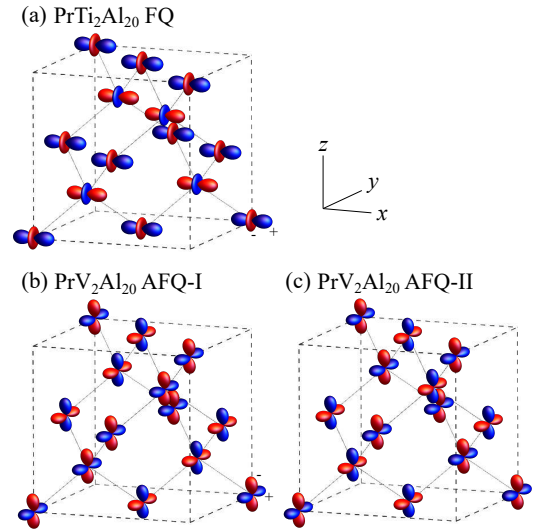


Fig. 6. (color online) Schematic configurations of the order parameters on the diamond lattice consist of Pr ions representing the O_2^0 -type FQ order (a) in the case of $\text{PrTi}_2\text{Al}_{20}$ and the O_2^2 -type AFQ orders, the high temperature AFQ-I (b) and the low temperature AFQ-II (c) in the case of $\text{PrV}_2\text{Al}_{20}$. \pm indicates the sign of the charge distribution.

type FQ order with the principal x -axis as shown in Fig. 6 (a), where the order parameter changes its sign between the Pr site 1 and 2 in the same unit cell as mentioned above. The O_2^0 -type FQ order is consistent with the neutron scattering and the ultrasonic experiments^{4,10)} but its sign is inconsistent with the NMR experiment¹¹⁾ which revealed that the O_2^0 order parameters of the Pr site 1 and 2 have the same sign in contrast to the present result with the opposite sign. This discrepancy will be discussed later. The T -dependence of the order parameter seems to show the 2nd-order phase transition (see Fig. 5 (a)) as observed in experiments,⁵⁾ however, it actually exhibits the 1st-order phase transition with a tiny discontinuity ~ 0.01 which is hard to detect as consistent with the prediction from the Landau theory.¹⁶⁾ We also explicitly calculate the specific heat (not shown) and confirm that the calculated result well accounts for the observed one⁵⁾ except for a tiny latent heat.

In the case of $\text{PrV}_2\text{Al}_{20}$ shown in Fig. 5 (b), the system exhibits two distinct AFQ orders, the high temperature AFQ-I and the low temperature AFQ-II, and shows subsequent two phase transitions, the 2nd-order one from normal to the AFQ-I

and the 1st-order one from the AFQ-I to the AFQ-II. This may be responsible for the double transitions observed by specific heat measurements¹⁵⁾ although the 1st-order phase transition has not been detected. The order parameters of the AFQ-I are the same signs between the Pr site 1 and 2 in the same unit cell, that is due to the large positive value of the site-diagonal components of the RKKY interactions at the $\mathbf{q} = (\pi/a, 0, \pi/a)$ as shown in Fig. 4 (d), while those of the AFQ-II are the opposite signs as shown in Fig. 5 (b). The linear combinations of the obtained order parameters $\langle \hat{O}_2^0 \rangle$ and $\langle \hat{O}_2^2 \rangle$ yield the O_2^2 -type AFQ orders with the principal x -axis for the both AFQ-I and AFQ-II as shown in Fig. 6 (b) and (c), where the order parameters are the same (opposite) signs between the Pr site 1 and 2 in the same unit cell resulting in the stripe-like (staggered-like) AFQ order for AFQ-I (AFQ-II). The O_2^2 -type AFQ order is observed in $\text{PrIr}_2\text{Zn}_{20}$,¹²⁾ although the quadrupole moment of the AFQ order in $\text{PrV}_2\text{Al}_{20}$ has not been determined by experiments so far.

4. Summary and Discussions

In summary, we have investigated the multipole orders in $\text{PrTi}_2\text{Al}_{20}$ and $\text{PrV}_2\text{Al}_{20}$ on the basis of the RKKY interactions between the quadrupoles \hat{O}_2^0 and \hat{O}_2^2 and the octupole \hat{T}_{xyz} of the Pr ions evaluated from the first-principles band calculations. What we have found are: In the case of $\text{PrTi}_2\text{Al}_{20}$, the 1st-order phase transition to the O_2^0 FQ order with a tiny discontinuity takes place. In the case of $\text{PrV}_2\text{Al}_{20}$, the system exhibits two distinct O_2^2 AFQ orders, the high temperature stripe-like AFQ-I and the low temperature staggered-like AFQ-II, and shows subsequent two phase transitions, the 2nd-order one from the normal to the AFQ-I and the 1st-order one from the AFQ-I to the AFQ-II. The octupole moment is absent in the both cases. The obtained results seem to be consistent with the experimental observations.

Detailed analysis has revealed that the maximum in the RKKY interaction $J_{\alpha\beta}^{\mu\nu}(\mathbf{q})$ at $\mathbf{q} = (0, 0, 0)$ in the case of $\text{PrTi}_2\text{Al}_{20}$ is mainly due to the small circular hole FSs centered at the Γ point. In the case of $\text{PrV}_2\text{Al}_{20}$, the number of electron relatively increases and the Fermi level shifts upward, resulting in the disappear of the small hole FSs and then the absence of the maximum in $J_{\alpha\beta}^{\mu\nu}(\mathbf{q})$ at $\mathbf{q} = (0, 0, 0)$. This is nothing but the origin of the difference between the FQ order of $\text{PrTi}_2\text{Al}_{20}$ and the AFQ order of $\text{PrV}_2\text{Al}_{20}$. We have also performed the first-principles band calculations for $\text{LaT}_2\text{Zn}_{20}$ ($T=\text{Ir, Rh}$) and have found that there are no small circular FSs similar to the case of $\text{PrV}_2\text{Al}_{20}$. This is consistent with the experiments where $\text{PrT}_2\text{Zn}_{20}$ ($T=\text{Ir, Rh}$) as well as $\text{PrV}_2\text{Al}_{20}$ exhibit the AFQ orders⁶⁻⁹⁾ while $\text{PrTi}_2\text{Al}_{20}$ exclusively exhibits the FQ order^{4,5)} among the Pr 1-2-20 systems.

In the present study, we have considered the c - f hybridization only between the $5d$ and $4f$ on the same Pr atom as the Pr $5d$ electrons give the dominant contribution to the susceptibility, and have neglected the inter-site c - f hybridizations between the Pr- $4f$ and the other c -electrons such as the Al- $3p$. We have also exclusively considered the non-Kramers Γ_3 CEF ground states of the Pr ions with the $4f^2$ configuration and have neglected the CEF excited states such as the magnetic Γ_4 and Γ_5 states which are considered to be important as the intermediate virtual states.¹⁸⁾ The discrepancy between the present study and the NMR experiment¹¹⁾ concerning the sign of the order parameters between the Pr site 1 and

2 in $\text{PrTi}_2\text{Al}_{20}$ may be resolved by including those effects neglected here, but the essential feature of the FQ and the AFQ orders obtained from the present study are expected to be unchanged.

Below T_Q , the superconductivity are found to coexist with the FQ and the AFQ orders for $\text{PrTi}_2\text{Al}_{20}$ and $\text{PrV}_2\text{Al}_{20}$, respectively^{8,9,13,14)} and are expected to be mediated by the quadrupole waves (quadrupolons) instead of the phonons in the BCS theory. Therefore, we need further calculations to obtain the quadrupole wave dispersions³⁷⁾ responsible for the pairing interaction and also for various physical quantities such as the power-law behavior of the specific heat.¹⁵⁾ Such calculations are now under way and explicit results will be reported in a subsequent paper.

Acknowledgments

This work was partially supported by JSPS KAKENHI Grant Number JP 21K03399. Numerical calculations were performed in part using OFP at the CCS, University of Tsukuba and the MASAMUNE-IMR, Tohoku University.

- 1) T. Onimaru and H. Kusunose, J. Phys. Soc. Jpn. **85**, 082002 (2016).
- 2) S. Niemann and W. Jeitschko, J. Solid State Chem. **114**, 337 (1995).
- 3) F. C. Frank and J. S. Kasper, Acta Cryst. **11**, 184 (1958).
- 4) M. Koseki, Y. Nakanishi, K. Deto, G. Koseki, R. Kashiwazaki, F. Shichinomiya, M. Nakamura, M. Yoshizawa, A. Sakai, and S. Nakatsuji, J. Phys. Soc. Jpn. **80**, SA049 (2011).
- 5) A. Sakai and S. Nakatsuji, J. Phys. Soc. Jpn. **80**, 063701 (2011).
- 6) I. Ishii, H. Muneshige, Y. Suetomi, T. K. Fujita, T. Onimaru, K. T. Matsumoto, T. Takabatake, K. Araki, M. Akatsu, Y. Nemoto, T. Goto, and T. Suzuki, J. Phys. Soc. Jpn. **80**, 093601 (2011).
- 7) I. Ishii, H. Muneshige, S. Kamikawa, T. K. Fujita, T. Onimaru, N. Nagasawa, T. Takabatake, T. Suzuki, G. Ano, M. Akatsu, Y. Nemoto, and T. Goto, Phys. Rev. B **87**, 205106 (2013).
- 8) T. Onimaru, K. T. Matsumoto, Y. F. Inoue, K. Umeo, Y. Saiga, Y. Matsushita, R. Tamura, K. Nishimoto, I. Ishii, T. Suzuki, and T. Takabatake, J. Phys. Soc. Jpn. **79**, 033704 (2010).
- 9) T. Onimaru, N. Nagasawa, K. T. Matsumoto, K. Wakiya, K. Umeo, S. Kittaka, T. Sakakibara, Y. Matsushita, and T. Takabatake, Phys. Rev. B **86**, 184426 (2012).
- 10) T. J. Sato, S. Ibuka, Y. Nambu, T. Yamazaki, T. Hong, A. Sakai, and S. Nakatsuji, Phys. Rev. B **86**, 184419 (2012).
- 11) T. Taniguchi, M. Yoshida, H. Takeda, M. Takigawa, M. Tsujimoto, A. Sakai, Y. Matsumoto, and S. Nakatsuji, J. Phys. Soc. Jpn. **85**, 113703 (2016).
- 12) K. Iwasa, K. T. Matsumoto, T. Onimaru, T. Takabatake, J. Mignot, and A. Gukasov, Phys. Rev. B **95**, 155106 (2017).
- 13) A. Sakai, K. Kuga, and S. Nakatsuji, J. Phys. Soc. Jpn. **81**, 083702 (2012).
- 14) M. Tsujimoto, Y. Matsumoto, T. Tomita, A. Sakai, and S. Nakatsuji, Phys. Rev. Lett. **113**, 267001 (2014).
- 15) M. Tsujimoto, Y. Matsumoto, and S. Nakatsuji, J. Phys., Conf. Ser. **592**, 012023 (2015).
- 16) T. Taniguchi, K. Hattori, M. Yoshida, H. Takeda, S. Nakamura, T. Sakakibara, M. Tsujimoto, A. Sakai, Y. Matsumoto, S. Nakatsuji, and M. Takigawa, J. Phys. Soc. Jpn. **88**, 084707 (2019).
- 17) S. Kittaka, T. Taniguchi, K. Hattori, S. Nakamura, T. Sakakibara, M. Takigawa, M. Tsujimoto, A. Sakai, Y. Matsumoto, and S. Nakatsuji, J. Phys. Soc. Jpn. **89**, 043701 (2020).
- 18) K. Hattori, and H. Tsunetsugu, J. Phys. Soc. Jpn. **83**, 034709 (2014).
- 19) S. Nagashima, T. Nishiwaki, A. Otani, M. Sakoda, E. Matsuoka, H. Harima, and H. Sugawara, JPS Conf. Proc. **3**, 011019 (2014).
- 20) M. Matsushita, J. Sakaguchi, Y. Taga, M. Ohya, S. Yoshiuchi, H. Ota, Y. Hirose, K. Enoki, F. Honda, K. Sugiyama, M. Hagiwara, K. Kindo, T. Tanaka, Y. Kubo, T. Takeuchi, R. Settai, and Y. Ōnuki, J. Phys. Soc. Jpn. **80**, 074605 (2011).
- 21) M. A. Ruderman and C. Kittel, Phys. Rev. **96**, 99 (1954).

- 22) T. Kasuya, Prog. Theor. Phys. **16**, 45 (1956).
- 23) K. Yosida, Phys. Rev. **106**, 893 (1957).
- 24) K. Hanzawa, J. Phys. Soc. Jpn. **84**, 024717 (2015).
- 25) T. Yamada, and K. Hanzawa, J. Phys. Soc. Jpn. **88**, 084703 (2019).
- 26) Y. Iizuka, T. Yamada, K. Hanzawa, and Y. Ōno, JPS Conf. Proc. **30**, 011152 (2020).
- 27) P. Blaha, K. Schwarz, G. Madsen, D. Kvasnicka, and J. Luitz, *WIEN2k, An Augmented Plane Wave + Local Orbitals Program for Calculating Crystal Properties* (Tech. Universität Wien, Vienna, 2001).
- 28) M. J. Kangas, D. C. Schmitt, A. Sakai, S. Nakatsuji, and J. Y. Chan, J. Solid State Chem. **196**, 274281 (2012).
- 29) P. Swateka, M. Kleinerta, P. Wisniewskia, and D. Kaczorowska, Comp. Mat. Sci. **153**, 461 (2018).
- 30) J. Kuneš, R. Arita, P. Wissgott, A. Toschi, H. Ikeda, and K. Held, Comput. Phys. Commun. **181**, 1888 (2010).
- I. Souza, N. Marzari, and D. Vanderbilt, Phys. Rev. B **65**, 1 (2002).
- 31) K. Hanzawa, J. Phys. Soc. Jpn. **80**, 023707 (2011).
- 32) When Ti is substituted by V in $\text{PrT}_2\text{Al}_{20}$ ($T=\text{Ti}, \text{V}$), the Fermi level ε_F shifts upward as shown in Figs. 2 (a) and (b) and then D_+ (D_-) given in eq. (4) (eq. (5)) increases (decreases) resulting in the increase in D_+/D_- . Therefore, D_+/D_- for $\text{PrTi}_2\text{Al}_{20}$ is set to be smaller than that for $\text{PrV}_2\text{Al}_{20}$.
- 33) The absolute values of $J_{\alpha\beta}^{iiv}$ show maximum for the 15th nearest neighbor sites in the both cases of (c) and (d).
- 34) T. Ito, W. Higemoto, K. Ninomiya, H. Luetkens, C. Baines, A. Sakai, and S. Nakatsuji, J. Phys. Soc. Jpn. **80**, 113703 (2011).
- 35) T. Ito, W. Higemoto, A. Sakai, M. Tsujimoto, and S. Nakatsuji, Phys. Rev. B **92**, 125151 (2015).
- 36) The discontinuity depends on the value of D_+/D_- , e. g., about 0.1 for $D_+/D_- = 0.5$ and 0.2 for $D_+/D_- = 0.4$.
- 37) R. Shiina, H. Shiba, P. Thalmeier, A. Takahashi, and O. Sakai, J. Phys. Soc. Jpn. **72**, 1216 (2003).